Available online at www.sciencedirect.com
SCIENCE DIRECT
Journal of Power Sources 154 (2006) 1–7
JOURNAL OF POWER SOURCES
www.elsevier.com/locate/jpowsour

Effect of solute dispersion on microstructure and electrical conductivity of $Ce_{0.85}Y_{0.13}Pr_{0.02}O_{2-\delta}$ solid electrolyte

S.K. Tadokoro, E.N.S. Muccillo *

Centro Multidisciplinar Para o Desenvolvimento de Materiais Cerâmicos, Instituto de Pesquisas Energéticas e Nucleares, CCTM, C.P. 11049, Sao Paulo 05422-970, SP, Brazil

Received 16 February 2005; accepted 14 March 2005
Available online 13 June 2005

Abstract

Solid solutions of $Ce_{0.85}Y_{0.13}Pr_{0.02}O_{2-\delta}$ were prepared by the co-precipitation and mixing of powder techniques and characterized by several techniques. The main purpose of this work was to evaluate the effect of the minority solute dispersion on the microstructure and electrical conductivity of this solid electrolyte. Praseodymium oxide co-doping of ceria–yttria produces changes in the crystallite size and in the average grain size of sintered pellets. Microstructural characterization shows that solid electrolytes with high homogeneity were obtained by the co-precipitation technique. Energy dispersive analysis and Raman spectroscopy results showed the formation of a Pr-rich solid solution of cerium oxide and praseodymium oxide in specimens prepared by the mixing of powder technique. Impedance spectroscopy results are dependent on the microstructure and show significant differences in the intergranular conductivity of sintered pellets prepared by different methods.

Keywords: Solid electrolyte; Ceria; Co-doping; Microstructure; Impedance spectroscopy

1. Introduction

Over the last several years, efforts have been made to lower the operating temperature of solid oxide fuel cells to the so-called intermediate temperature (<750 °C) range. This goal has contributed to the discovering and designing of new oxide–ion conductors, and recent reviews on this subject may be found in the literature [1,2]. At present, however, the most developed electrolytes with sufficient electrical properties to operate in that temperature range are those based on doped ceria. Yttrium and rare-earth-doped ceria solid electrolytes are better ionic conductors than yttria-stabilized zirconia, and may operate at temperatures lower than 700 °C with good fuel cell efficiency [3–6].

A number of cations may be incorporated into the cubic fluorite-type lattice of ceria solid electrolytes as co-dopants, and their effects have been recently studied. One of the most investigated co-dopant in ceria solid solutions is praseodymium [7–15]. The co-doping of ceria ceramics with praseodymium oxide was initially proposed to increase the ionic conductivity and to decrease the electronic conductivity of doped-ceria materials, aiming to increase the electrolytic domain of the solid electrolyte [7,8]. Some further studies, however, did not confirm that effect [9,10]. Moreover, the thermal expansion coefficient was shown to increase with praseodymium oxide co-doping [11]. An increase in the p-type electronic conductivity was observed for small praseodymium oxide additions to gadolinia-doped ceria [12,13]. Increase of the ionic conductivity in samaria-doped ceria was recently claimed as a consequence of praseodymium oxide incorporation [14]. In addition to the effects of this oxide material on electrical conductivity of doped ceria solid electrolytes, it was demonstrated that it increases the tendency for segregation of the rare-earth dopant at the grain boundaries [15]. In these studies, microstructure-related properties were evaluated in solid solutions prepared by different methods

* Corresponding author. Tel.: +55 11 38169343; fax: +55 11 38169370.
E-mail address: enavarro@usp.br (E.N.S. Muccillo).

0378-7753/$ – see front matter © 2005 Elsevier B.V. All rights reserved.
doi:10.1016/j.jpowsour.2005.03.194

without mention on the chemical homogeneity of solid solutions.

In this work, solid solutions of $Ce_{0.85}Y_{0.13}Pr_{0.02}O_{2-\delta}$ were studied by several techniques to evaluate the effect of a minority solute dispersion on the microstructure and the electrical conductivity of this solid electrolyte.

2. Experimental procedure

2.1. Sample preparation

$Ce(NO_3)_3{\cdot}6H_2O$ (99.99%, Aldrich), Y_2O_3 (99.99%, Sigma Chem. Co.) and Pr_6O_{11} (99.9%, Aldrich) were used as starting materials. A stock solution of cerium nitrate was prepared in deionized water. Stock solutions of yttrium and praseodymium nitrates were prepared by dissolving the corresponding oxides in nitric acid solutions under heating and stirring. The concentration of these solutions was controlled by gravimetry.

Solid solutions of composition $Ce_{0.85}Y_{0.13}Pr_{0.02}O_{2-\delta}$ were prepared by two methods of synthesis: co-precipitation, CP and mixing of powders, MP. The co-precipitation method involved the simultaneous precipitation of cerium, yttrium and praseodymium hydroxides. The addition of the cation solution to an ammonium hydroxide solution resulted in the formation of a precipitate, which was washed with a diluted solution of ammonium hydroxide for elimination of anions, followed by a sequence of washings with different media for partial dehydration of the precipitate. The complete dehydration sequence consisted of washings with alcoholic solutions (absolute ethanol and isopropyl alcohol), and azeotropic distillation with *n*-butyl alcohol. Finally, the co-precipitate was dried at 45 °C. The yield (∼90%) with this method was higher than that of oxalate co-precipitation [16]. The preparation of the solid solution by the mixing of powders method consisted of the co-precipitation of cerium and yttrium hydroxides, using the same experimental conditions as in the case of the co-precipitation method and after drying the co-precipitate was mixed with a suitable amount of Pr_6O_{11}. The mixture was carefully homogenized in an agate mortar for 10 min.

The single-doped $Ce_{0.85}Y_{0.15}O_{2-\gamma}$ solid solution, hereafter called the "standard composition", was also synthesized by the hydroxide co-precipitation technique and characterized by different methods for comparison purposes.

Powders prepared by the two techniques were calcined, pressed into pellets and sintered at 1450 °C for 4 h with heating and cooling rates of 5 °C min^{-1}.

2.2. Sample characterization

The thermal decomposition behavior of dried powders was studied by simultaneous thermogravimetry, TG and differential thermal analysis, DTA (STA409, Netzsch), heating at a rate of 5 °C min^{-1} up to 1000 °C under synthetic air. Alumina (Alumalux, Alcoa) was used as a reference material. Phase characterization and crystallite size determination were done by X-ray diffraction, XRD (D8 Advance, Bruker-AXS) experiments using a Ni-filtered Cu Kα radiation. Typical experimental conditions were 40 kV and 40 mA. Scans were conducted in the range, $20^\circ \le 2\theta \le 80^\circ$ with 0.05° per 2 s for phase characterization and in the range, $25^\circ \le 2\theta \le 31^\circ$ with 0.01° per 5 s for crystallite size, t_{XRD}, determination. Values of crystallite size were estimated by the Scherrer equation: $t_{XRD} = 0.9\lambda/B^{1/2}\cos\theta$, where λ is the wavelength of the X-rays and θ is the diffraction angle. In these calculations, it was assumed a Gaussian peak-shape, and the instrumental broadening was corrected using high-grade Si powder as standard.

Additional structural characterization of samples was performed with Raman spectroscopy (Model 3000, Renishaw Raman microscope coupled to an Olympus BH-2 optical microscope). The exciting radiation of a He–Ne laser (model 127, Spectra Physics) at 632.8 nm was used in the 250–1000 cm^{-1} spectral range. Some microstructural aspects of sintered pellets were observed by scanning electron microscopy, SEM (JXA 6400, Jeol and XL30, Philips) on polished and thermally etched surfaces. SEM observations were performed on the internal (frature) surface. Average grain size, *G*, values were estimated by the intercept method [17]. Energy dispersive spectroscopy (EDS) was used for elemental analysis in micro-regions of sintered pellets.

Silver paste was used as electrode material for electrical measurements. Electrical resistance, *R*, measurements were carried out on sintered pellets by impedance spectroscopy using a LF impedance analyzer (4192A, Hewlett Packard) in the 5 Hz to 13 MHz frequency range with an applied ac signal of 50 mV. Data were analyzed in the impedance mode using a special computer program [18]. Results of electrical measurements are plotted as the imaginary ($-Z''$) versus the real (Z') part of the impedance, normalized for sample dimensions. No correction for specimen porosity was carried out. The electrical conductivity, σ, was then calculated from the measured resistance allowing for obtaining Arrhenius plots according to: $\sigma = \sigma_0 \exp(-E/kT)$, where *E* is the apparent activation energy for conduction, *k* the Boltzmann constant, *T* the absolute temperature and σ_0 the pre-exponential factor.

In the temperature range (200–400 °C) of measurements, impedance diagrams show two semicircles related to the electrical response of the solid electrolyte. The high-frequency semicircle is due to the conduction process across grains (intragranular, g), whereas the low-frequency semicircle is related to the blocking of charge carriers at grain interfaces (intergranular, ig).

3. Results and discussion

3.1. Thermal decomposition

Fig. 1 shows thermal analysis results obtained for dried powders. From TG curves (Fig. 1a), the total weight loss up to 1000 °C is around 16%. The theoretical weight loss

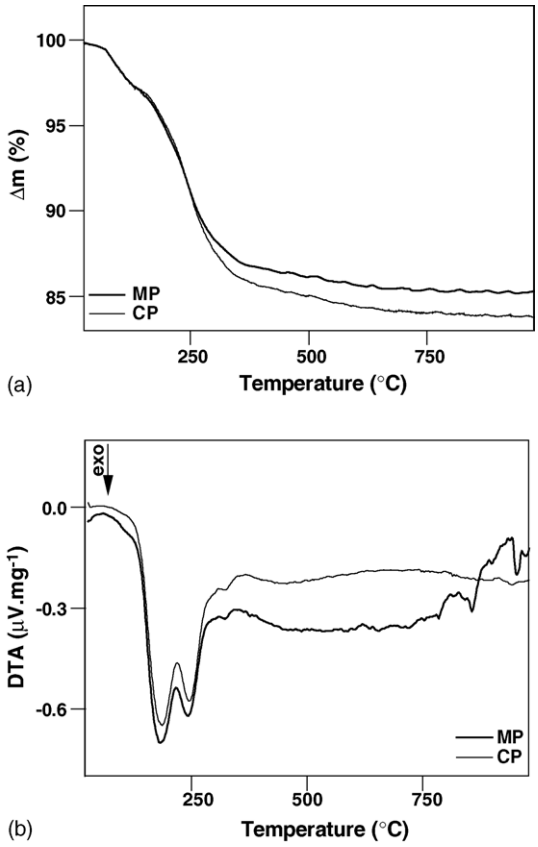

Fig. 1. Thermogravimetric (a) and differential thermal analysis (b) curves of dried materials.

depends on the type of hydroxide formed ($Ce(OH)_3$ and/or $Ce(OH)_4$) and on the degree of hydration. The weight loss is due to several reactions: elimination of physically adsorbed water and crystallization water, evolution of alcohol residues adsorbed onto particle surfaces, loss of constitution water and formation of the product material. The small difference in the total weight loss in these curves is attributed to the thermal decomposition of praseodymium hydroxide, in the case of the co-precipitated material. It may be noted that the weight loss is negligible for temperatures higher than 400 °C, and this temperature was chosen for calcination of dried gels.

DTA curves (Fig. 1b) for both materials exhibit similar thermal events up to ∼750 °C. The endothermic peak at low temperature (<100 °C) is related to the loss of water. The three exothermic peaks detected at ∼200, ∼250 and ∼330 °C are assigned to hydroxide decomposition, elimination of organic material and oxide crystallization, respectively. The DTA curve for the material prepared by the mixing of Pr_6O_{11} to the co-precipitated powder presents, in addition, two exothermic peaks at ∼860 and ∼950 °C. It is known [19] that praseodymium oxides belong to a homologous series Pr_nO_{2n-2} of intermediate phases with narrow ranges of non-stoichiometry and with ordered compounds. The end members of this series are $PrO_{1.5}$ and PrO_2. Therefore, these DTA peaks at high temperatures are related to compositional phase changes of the praseodymium oxide.

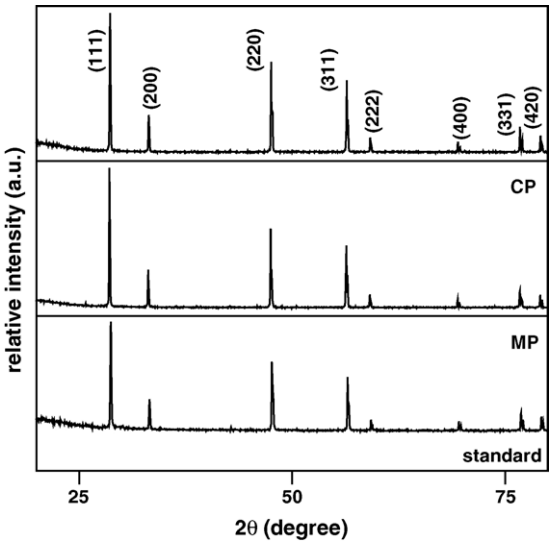

Fig. 2. X-ray diffraction patterns of co-doped and the standard composition sintered pellets.

3.2. Structural and microstructural characterization

Fig. 2 shows X-ray diffraction patterns obtained after calcination of gels at 400 °C for 2 h, pressing and sintering at 1450 °C for 4 h. These diffractograms are almost unchanged with that of pure ceria (ICDD 34-394). The diffraction peaks are sharp and no reflections were observed that could be attributed to isolated yttrium oxide or to spurious phases. Values of crystallite size estimated for the most intense reflection are shown in Table 1.

The crystallite size of specimens prepared by co-precipitation is higher than that of the standard composition. In contrast, pellets prepared by mixing of praseodymium oxide with the co-precipitate of ceria–yttria have a lower crystallite size value. As can be seen, the synthesis route leads to different values of crystallite size. This is a first indication that the process of incorporation of a minority solute into the ceria matrix influences the solid solution formation.

Fig. 3 shows representative SEM micrographs of sintered pellets prepared by mixing of powders (Fig. 3a) and co-precipitation (Fig. 3b). The main microstructural characteristics are grains with uniform morphology and large distribution of grain sizes. Average values of grain sizes are quite similar, as shown in Table 1.

It is worth noting in these micrographs negligible porosity, either intragrain or intergrain, although the sintering temperature was lower than that usually employed to obtain high

Table 1
Values of crystallite size (t_{XRD}) and average grain size (G) of sintered pellets

Specimen	t_{XRD} (nm)	G (μm)
$Ce_{0.85}Y_{0.15}O_{2-\gamma}$	101.1	1.6
$Ce_{0.85}Y_{0.13}Pr_{0.02}O_{2-\delta}$ – MP	91.4	1.3
$Ce_{0.85}Y_{0.13}Pr_{0.02}O_{2-\delta}$ – CP	116.0	1.4

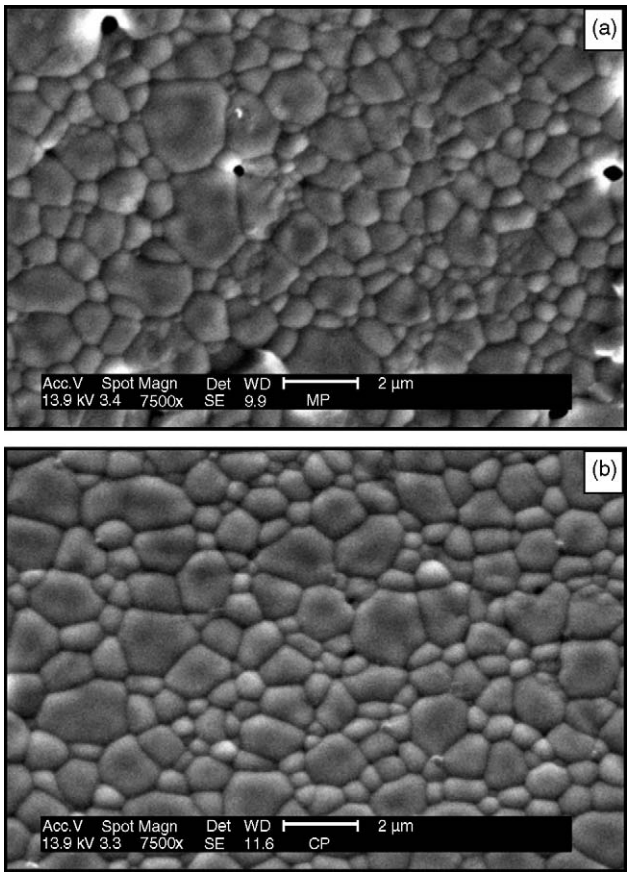

Fig. 3. SEM micrographs of sintered pellets prepared by mixing of powders (a) and co-precipitation (b).

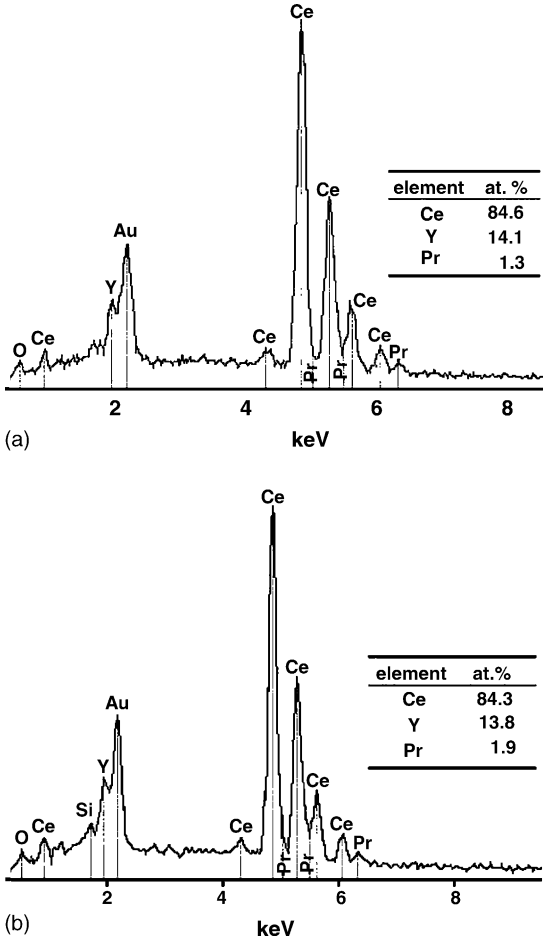

Fig. 4. EDS spectra of co-doped sintered pellets: MP (top) and CP (bottom).

densification in doped ceria ceramics [20]. This result shows the relatively high sinterability of these powders.

To determine the actual contents of Ce, Y and Pr in these samples, they were analyzed by EDS coupled to a scanning electron microscope. Fig. 4 shows EDS spectra of sintered pellets and results of the elemental analysis, which are averaged values over three independent determinations.

These figures are in good agreement with nominal cation contents: Ce = 85 at.%, Y = 13 at.% and Pr = 2 at.%.

During microstructural observations, however, some micro-regions with a different morphology were also seen in those pellets prepared from mixing of powders. Fig. 5 shows a low-magnification SEM micrograph where two of these regions may be visualized. The morphology observed is typical of a ceramic in which a local expansion occurred. In most cases, the expansion and the resulting surface disruption are due to the release of gases entrapped inside the pellet or to a phase transition accompanied by volume variation.

Some of these regions were analyzed by EDS and results are shown in Fig. 6. The EDS spectra and the elemental analysis demonstrate that the praseodymium oxide was not randomly distributed by the mixing of powders method, but concentrated in small regions forming a praseodymium-rich solid solution with cerium oxide. It was recently reported [15] the segregation observed at grain boundaries of a praseodymium-rich phase in ceramics of ceria co-doped with gadolinium and praseodymium oxides, prepared by mixing of powders. In that case, the segregated phase spread out along the grain boundaries and results of energy dispersive analysis indicated an enrichment of Pr and Gd

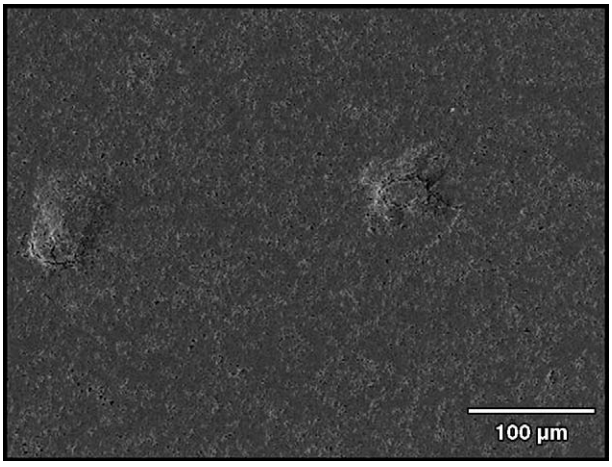

Fig. 5. Low-magnification SEM micrograph obtained for the material prepared by mixing of powders.

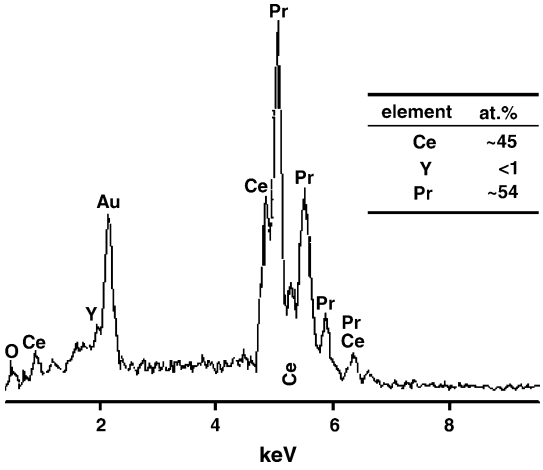

Fig. 6. EDS spectrum of expanded micro-regions.

in comparison with the bulk composition. In effect, the tendency for segregation at grain boundaries of gadolinium in doped ceria was earlier observed by electron energy-loss spectroscopy [21], and the effect of praseodymium was to increase the tendency for solute segregation. In this case, however, the segregated phase remained isolated and it is composed of the minority solute and cerium oxide.

To obtain a better insight into the structure of the segregated phase, pellets prepared by the two methods of synthesis were analyzed by Raman spectroscopy. Fig. 7 shows optical micrographs taken of the cross-sectional area of pellets during sample focalization for spectroscopic analysis. Specific regions of these samples chosen for this analysis are indicated by arrows. The optical micrograph obtained for the material prepared from the co-precipitated powder (top) has a homogeneous but rough surface. The surface of the pellet prepared by mixing of powders (bottom) presents, in addition, regions with dark contrast. In what follows it is designated A regions with bulk characteristics, and B those micro-regions with dark contrast.

Fig. 8 shows Raman spectra of sintered samples prepared from co-precipitated powders (a), and by mixing of powders (b and c). The Raman spectrum representing the bulk (region A) of pellets (Fig. 8a and b) displays a relatively sharp band with maximum amplitude near 467 cm^{-1}. This band is related to the T_{2g} vibrational mode typical of the cubic structure. In addition, these spectra exhibit two low-intensity bands at ~520 and ~650 cm^{-1}, which are attributed to oxygen vacancies generated as charge compensating defects [22]. Therefore, the bulk solid solution has a single cubic fluorite-type structure. The Raman spectrum of region B (Fig. 8c) shows two bands with maximum amplitudes at ~455 and ~570 cm^{-1}. The low-wavenumber band is also related to the T_{2g} vibrational mode of the cubic structure. The apparent displacement of its maximum amplitude towards lower wavenumbers is partially attributed to the increased background in this spectral range. The high-wavenumber Raman band at 570 cm^{-1} may be identified with results of a previous

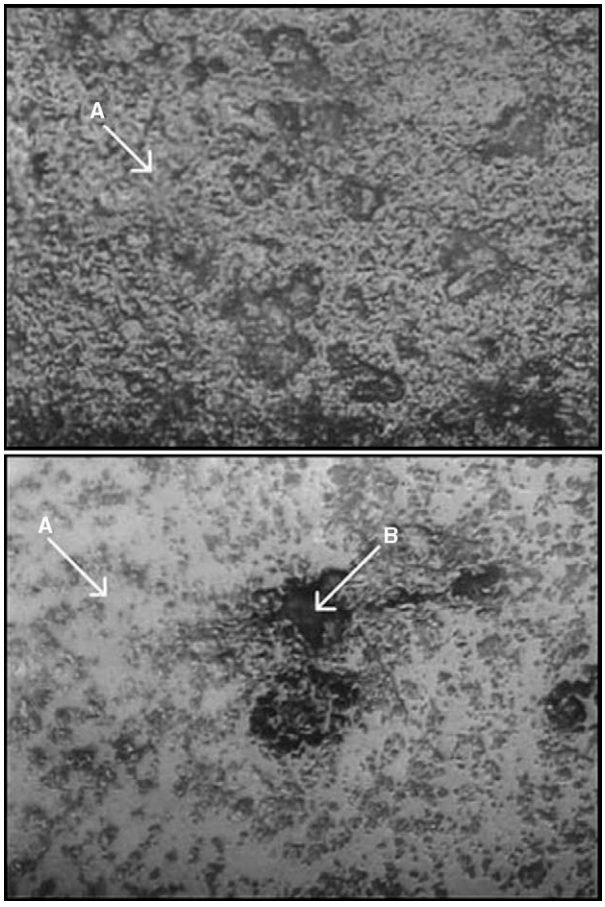

Fig. 7. Images of co-doped pellets surfaces obtained in an optical microscope. Magnification, 80×.

work on ceria doped with rare-earth elements, as a consequence of the solid solution formation between cerium oxide and praseodymium oxide [22]. According to these authors, increasing the praseodymium content results in an increase of the maximum amplitude of this Raman band.

It must be emphasized that the different morphology of pellets prepared by the mixing of powders was observed

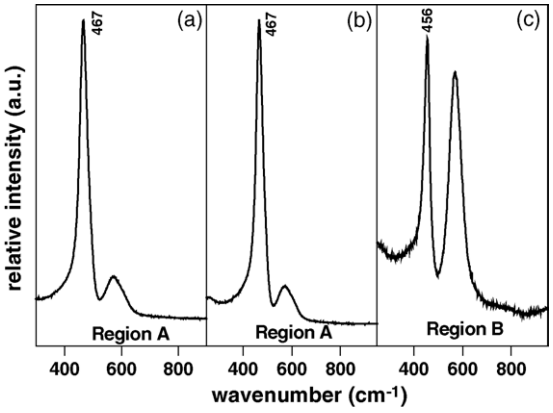

Fig. 8. Raman spectra of sintered pellets prepared with co-precipitated material (a) and by mixing of powders (b and c).

only after thermal etching. According to literature data [23] solid solutions of $Ce_{1-x}Pr_xO_{2-\gamma}$ with $x > 0.2$ decompose into two fluorite-type phases once the specimen is heat treated at temperatures higher than 800 °C in air. Therefore, the Pr-rich solid solution formed during sintering of pellets should undergo a phase transition in the subsequent thermal treatment giving rise to the observed surface relief.

These results demonstrate that the method of synthesis may give rise to differences in both structure and microstructure of sintered ceramics, which may not be observed by some characterization techniques due to experimental limitations.

3.3. Impedance spectroscopy

In the entire temperature and frequency ranges of measurements, the electrical response of silver-electroded pellets gives rise to two well-resolved semicircles in impedance diagrams. As an example, Fig. 9 shows $-Z'' \times Z'$ plots of $Ce_{0.85}Y_{0.13}Pr_{0.02}O_{2-\delta}$ solid electrolytes prepared by different techniques and measured at 262 °C. For comparison purposes, the impedance diagram of the standard composition is also shown. Numbers over experimental points are the logarithm of the frequency, in Hz. Due to the large difference in the relative magnitudes of these semicircles they are shown as complete diagrams in Fig. 9a and as a zoom of the high-frequency range in Fig. 9b.

The low-frequency semicircle, assigned to the blocking effect of charge carriers at grain boundaries of the pellet prepared from co-precipitated powder, is higher than that of the standard composition. The decrease in the average grain size (see Table 1) due to praseodymium co-doping ceria may be one of the reasons for this effect. In contrast, for the

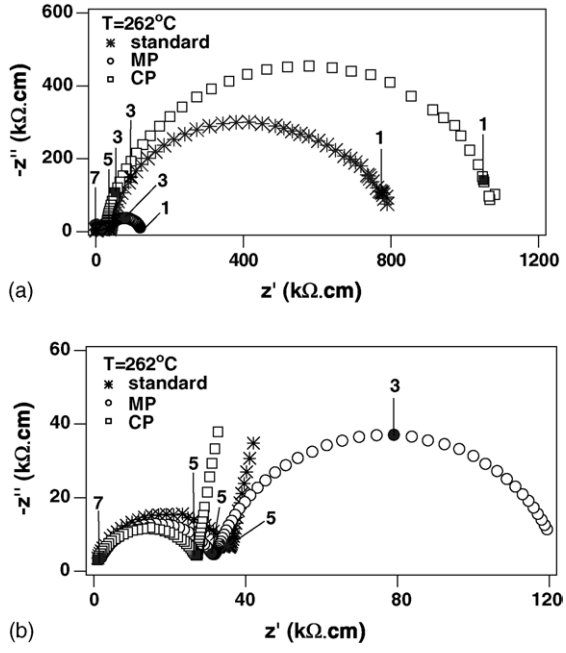

Fig. 9. Impedance diagrams of sintered pellets.

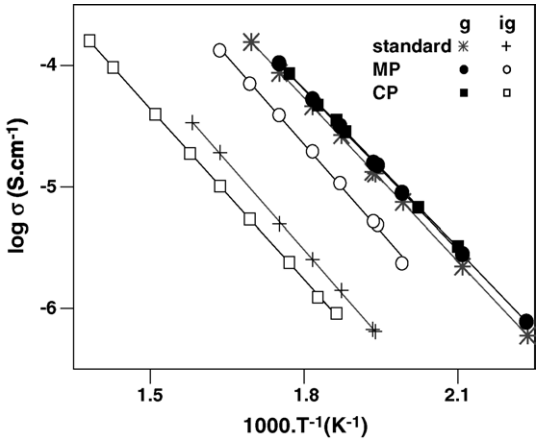

Fig. 10. Arrhenius plots of the electrical conductivity of sintered pellets.

pellet prepared by mixing of powders, the blocking effect is comparatively low. This result would be expected once this pellet has a different microstructure and may be thought of as a mixture of two solid solutions (ceria–yttria–praseodymia and ceria–yttria) with quite different electrical behaviors.

In the high-frequency range, the electrical resistivity of grains of co-doped pellets is slightly lower than that of the standard composition. Then, this result shows that the addition of small amounts of praseodymiun oxide to ceria–yttria improves the electrical response of grains. However, this small improvement should not be significant on a logarithm scale of the Arrhenius plots of conductivity.

Fig. 10 shows Arrhenius plots of the electrical conductivity of sintered pellets. The intragranular conductivity plots show no noticeable change of slope in the limited temperature range of the measurements. Apparent activation energy values obtained by curve fitting resulted in 0.87 eV for the standard composition, and 0.85 eV for co-doped pellets.

The intergranular conductivity of the pellet prepared with co-precipitated powder is less than one order of magnitude lower than that of the standard composition, mostly due to a higher grain boundary density. In contrast, the intergranular conductivity of the pellet prepared by mixing of powders is about one order of magnitude higher than that of the pellet prepared with co-precipitated material. Apparent activation energy values are in the 0.91–0.94 eV range.

The difference in magnitudes of the intergranular component of the conductivity may be explained as a microstructure-related effect. The formation of the solid solution between ceria and praseodymia in pellets prepared by mixing of powders must account for this effect.

4. Conclusions

Chemically homogeneous solid solutions of cerium, yttrium and praseodymium oxides were obtained by the hydroxide co-precipitation technique. The addition of small amounts (2 at.%) of praseodymium to yttria-doped ceria pro-

duces an increase of the crystallite size along with a decrease of the grain size in sintered pellets. Impedance spectroscopy results show a small increase of the intragranular conductivity compared to that of the single-doped material. The increase in the density of grain boundaries may account for most of the observed decrease in the intergranular conductivity.

Non-homogeneous solid solutions of praseodymium, yttrium and cerium oxides were obtained by the mixing of powder technique. Energy dispersive analysis and Raman spectroscopy show the formation of a Pr-rich solid solution between praseodymium oxide and cerium oxide. This secondary phase introduces substantial changes in the intergranular conductivity of the sintered pellets.

Acknowledgements

Authors acknowledge FAPESP (94/05929-5, 95/05172-4 and 96/09604-9), CNPq (300934/94-7) and CNEN for financial support, L.S. Montagna for EDS analysis and the molecular spectroscopy laboratory of IQ/USP for Raman experiments. S.K. Tadokoro acknowledges FAPESP (00/08908-1) for the scholarship.

References

[1] B.C.H. Steele, J. Mater. Sci. 36 (2001) 1053–1068.
[2] J.B. Goodenough, Ann. Rev. Mater. Res. 33 (2003) 91–128.
[3] T. Kudo, H. Obayashi, J. Electrochem. Soc. 123 (1976) 415–419.
[4] H. Inaba, H. Tagawa, Solid State Ionics 83 (1996) 1–16.
[5] B.C.H. Steele, Solid State Ionics 129 (2000) 95–110.
[6] C. Miliken, S. Guruswamy, A. Khandar, J. Am. Ceram. Soc. 85 (2002) 2479–2486.
[7] D.L. Maricle, T.E. Swarr, H.L. Tuller, US Patent No. 5,001,021, March 19 (1991).
[8] D.L. Maricle, T.E. Swarr, S. Karavolis, Solid State Ionics 52 (1992) 173–182.
[9] B.C.H. Steel, K. Zheng, R.A. Rudkin, N. Kiratzis, M. Christie, in: M. Dokiya, O. Yamamoto, H. Tagawa, S.C. Singhal (Eds.), Proceedings of the Fourth International Symposium on Solid Oxide Fuel Cells, vol. 95-1, The Electrochemical Society, USA, 1995, pp. 1028–1038.
[10] N. Maffei, A.K. Kuriakose, Solid State Ionics 107 (1998) 67–71.
[11] W. Huang, P. Shuk, M. Greenblatt, Solid State Ionics 113–115 (1998) 305–310.
[12] S. Lübke, H.D. Wiemhofer, Solid State Ionics 117 (1999) 229–243.
[13] V.V. Kharton, A.P. Viskup, F.M. Figueiredo, E.N. Naumovich, A.A. Yaremchenko, F.M.B. Marques, Electrochim. Acta 46 (2001) 2879–2889.
[14] X. Qi, Y.S. Lin, C.T. Holt, S.L. Swartz, J. Mater. Sci. 38 (2003) 1073–1079.
[15] V.V. Kharton, A.P. Viskup, F.M. Figueiredo, E.N. Naumovich, A.L. Shaulo, F.M.B. Marques, Mater. Lett. 53 (2002) 160–164.
[16] S.K. Tadokoro, T.C. Porfírio, R. Muccillo, E.N.S. Muccillo, J. Power Sources 130 (2004) 15–21.
[17] M.I. Mendelson, J. Am. Ceram. Soc. 52 (1969) 443–446.
[18] M. Kleitz, J.H. Kennedy, in: P. Vashista, J.N. Mundy, G.K. Shenoy (Eds.), Fast Ion Transport in Solids, Electrodes and Electrolytes, North-Holland, Amsterdam, 1979, pp. 185–186.
[19] B.G. Hyde, D.M.J. Bevan, L. Eyring, Philos. Trans. R. Soc. Lond. Ser. A 259 (1966) 583–614.
[20] J.V. Herle, T. Horita, T. Kawada, N. Sakai, H. Yokokawa, M. Dokiya, J. Am. Ceram. Soc. 80 (1997) 933–940.
[21] Y. Lei, Y. Ito, N.D. Browning, T.J. Mazanec, J. Am. Ceram. Soc. 85 (2002) 2359–2363.
[22] J.R. McBride, K.C. Hass, B.D. Poindexter, W.H. Weber, J. Appl. Phys. 76 (1994) 2435–2441.
[23] C. Ftikos, M. Nauer, B.C.H. Steele, J. Eur. Ceram. Soc. 12 (1993) 267–270.